HNUE JOURNAL OF SCIENCE
Natural Sciences 2024, Volume 69, Issue 2, pp. 90-97
This paper is available online at http://hnuejs.edu.vn/ns
DOI: 10.18173/2354-1059.2024-0023

THEORETICAL INVESTIGATION OF NITROGEN AND BORON DOPING EFFECTS ON THE ELECTRONIC AND OPTICAL PROPERTIES OF CERIA

Nguyen Hoang Hao[1], Truong Thi Binh Giang[1], Cao Hoang Minh Chau[1], Nguyen Thi Kim Giang[2] and Nguyen Thi Thu Ha[2,*]

[1]*Faculty of Chemistry, College of Education, Vinh University, Vinh city, Vietnam*
[2]*Faculty of Chemistry, Hanoi National University of Education, Hanoi city, Vietnam*
Corresponding author: Nguyen Thi Thu Ha, e-mail: ntt.ha@hnue.edu.vn

Received June 2, 2024. Revised June 20, 2024. Accepted June 27, 2024.

Abstract. This study investigates the impact of nitrogen (N) and boron (B) doping on the electronic structure and optical properties of ceria (CeO_2) using a combination of density functional theory plus U (DFT+U) and the GFN-xTB method. The calculations of electronic parameters and population analysis indicated that doping with N and B reduces the surface Lewis acidity of ceria, decreases the bandgap, and narrows the edges of the valence band and conduction band. These findings offer valuable insights into comprehending the photocatalytic performance of CeO_2-based materials.

Keywords: CeO_2, N doped CeO_2, B doped CeO_2.

1. Introduction

Ceria (CeO_2) has emerged as a prominent photocatalyst due to its unique electronic properties, high oxygen storage capacity, and excellent chemical stability. These characteristics make ceria a valuable material for a wide range of applications, including environmental remediation, water splitting, and the degradation of organic pollutants. The efficiency of ceria as a photocatalyst is largely determined by its ability to absorb light, generate electron-hole pairs, and facilitate charge transfer processes that drive photocatalytic reactions [1], [2]. Despite its promising attributes, pristine ceria faces certain limitations that hinder its photocatalytic performance. One major challenge is its wide bandgap, approximately 3.2 eV [3], which restricts its ability to absorb visible light. This limitation means that under solar irradiation, ceria can only utilize a small fraction of the solar spectrum, thus reducing its overall photocatalytic efficiency. Moreover, the high recombination rate of photogenerated electron-hole pairs in ceria further diminishes its photocatalytic activity, as it limits the availability of charge carriers for photocatalytic

reactions. To address these challenges, doping ceria with various elements has been extensively explored as a strategy to enhance its photocatalytic performance [4].

Among the various dopants, nitrogen, and boron have attracted significant attention. Doping ceria with nitrogen and boron introduces new energy levels within the band structure of ceria, which can effectively reduce its bandgap and extend its light absorption into the visible region of the solar spectrum [4]-[7]. This modification is crucial because visible light constitutes a significant portion of the solar spectrum, and its effective utilization is key to improving the overall efficiency of photocatalysts. Nitrogen doping is particularly interesting due to nitrogen's ability to introduce localized states near the valence band, which can narrow the band gap and enhance visible light absorption. Additionally, nitrogen doping can influence the electronic structure and improve the separation and migration of photogenerated charge carriers, thereby reducing the recombination rate of electron-hole pairs [4], [5]. Similarly, boron doping offers another pathway to modify the electronic properties of ceria. Boron can introduce acceptor states and alter the charge distribution within the ceria lattice [6], [7]. This can lead to improved charge carrier dynamics and potentially enhance photocatalytic activity by increasing the number of active sites available for catalytic reactions.

The motivation for this research lies in the potential to significantly enhance the photocatalytic efficiency of ceria by understanding and optimizing the effects of nitrogen and boron doping. By providing detailed theoretical insights into the electronic and optical changes induced by these dopants, this study aims to guide the design of more efficient ceria-based photocatalysts, contributing to advancements in sustainable energy and environmental technologies.

2. Content

2.1. Models and computational methods

The CeO_2 (111)-(3×3× 3) surface was employed to represent the CeO_2 substrate. The (111) surface of ceria was selected because it is the most stable, as demonstrated by the XRD pattern of CeO_2 [8]. All slabs were periodically replicated, with a vacuum gap of 15 Å. N-doped and B-doped CeO_2 structures were generated by replacing an oxygen atom in the first layer with a single nitrogen or boron atom (Figure 1).

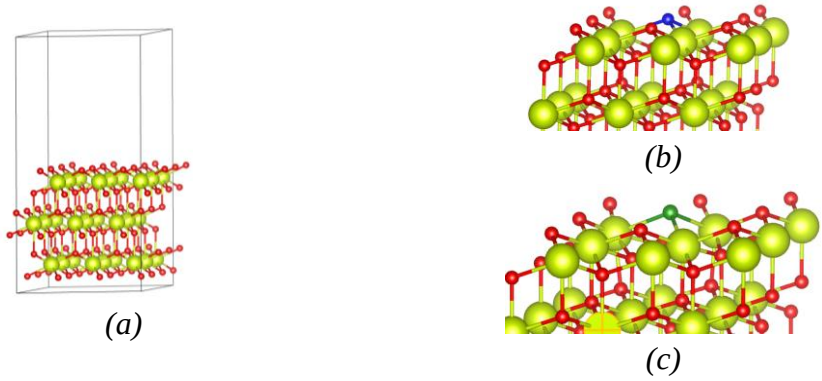

(a) *(b)* *(c)*

Figure 1. Models of CeO_2 (a), N doped CeO_2 (b) and B doped CeO_2 (c); color codes: yellow - cerium, red - oxygen, blue - nitrogen, green - boron

All optimization computations were carried out utilizing density functional theory (DFT) methodologies as implemented in the CP2K software [https://www.cp2k.org/]. The exchange-correlation potential was treated using the generalized gradient approximation (GGA) with the Perdew-Burke-Ernzerhof (PBE) spin-polarized functional [9]. Wavefunctions were expanded with a double-zeta valence polarized (DZVP) basis set, augmented by an auxiliary plane-wave basis with a cutoff energy of 250 Ry. Core electrons were represented by norm-conserving pseudopotentials [10]. Brillouin zone integration utilized a reciprocal space grid that included only the Γ-point. Dudarev's method for DFT+U calculations was applied to describe the Ce 4f electrons [11]. A U–J value of 8.0 eV was employed, corresponding to a simulated bandgap value of 3.18 eV for ceria. Additionally, van der Waals (vdW) interactions were incorporated using DFT-D calculations based on the Grimme D3 method to precisely estimate interaction forces [12].

Several parameters were calculated and analyzed to assess the electronic and optical properties of the N/CeO_2 and B/CeO_2 materials, including ionization potential energy (IP), electron affinity (EA), and band gap (E_g). The latter was calculated as the energy difference between the LUMO and HOMO of the studied systems. From the IP, EA, and E_g values, we evaluated the energies of the valence band (E_{VB}) and conduction band (E_{CB}) using the following formulas:

$$E_{VB} = \chi - E_e + 0.5E_g \quad (1)$$

$$E_{CB} = E_{VB} - E_g \quad (2)$$

where E_e = 4.5000eV is the energy of a free electron on the hydrogen scale, and χ is the absolute electronegativity calculated as: χ = (IP + EA)/2 with IP and EA representing the ionization potential and electron affinity, respectively.

Additionally, parameters such as the global electrophilicity index (GEI), which characterizes the Lewis acidity of the material surface, and the images of the frontier molecular orbitals (HOMO and LUMO), were analyzed to elucidate the impact of N and B doping on the electronic structure of ceria. All the electronic parameters IP, EA, and GEI of the studied system were calculated using the GFN-xTB method [13].

2.2. Results and discussions

Based on the optimized models of the CeO_2, N/CeO_2, and B/CeO_2 structures using the DFT+U method, various geometric parameters and Mulliken atomic charges are presented in Table 1. Additionally, the total bond order (BO) values between the N and B atoms and the Ce and O atoms are provided, with the values in parentheses representing the bond order between N/B and the three nearest Ce/O atoms.

In the pristine structure of ceria, oxygen atoms are symmetrically distributed, forming bonds with three cerium atoms, resulting in a total bond order of 1.476. Each oxygen atom carries a partial negative charge of -0.581 e. When oxygen is replaced by nitrogen or boron, this symmetry is disrupted, particularly in the case of boron. This disruption is evident from the variations in bond lengths and bond angles to the three nearest cerium atoms. Notably, when N and B substitute for O in the CeO_2 structure, they form bonds with both cerium and oxygen atoms. Consequently, the negative charge on nitrogen and

boron atoms is significantly reduced compared to the original replaced oxygen atom. Specifically, the charge on nitrogen is -0.227 e, meanwhile, the charge on boron is +0.442 e.

Table 1. Geometric parameters and atomic charges

System	d(X-Ce), Å	<CeXCe, degree	q(X), e	BO
CeO_2	2.345 - 2.346	109.25 - 109.33	-0.581	1.476 (O – Ce)
N/CeO_2	2.498; 2.508; 2.677	109.50; 100.41; 100.89	-0.227	1.632** (N–Ce: 0.913; N–O: 0.449)
B/CeO_2	2.891; 3.197; 3.198; 1.259*	81.58; 83.55; 83.42;	+0.442	1.807** (B–Ce: 0.674; B–O: 1.039)

*Note: X represents O, N, and B corresponding to CeO_2, N/CeO_2, and B/CeO_2, respectively; *: distance from B to the nearest O atom; **: the value outside the parentheses represents the total bond order of the doping atom with the atoms in CeO_2, while the values inside the parentheses denote the partial bond orders for each type of bond.*

This significant change in atomic charge is consistent with the calculated bond orders between N or B and the cerium and oxygen atoms in ceria. Nitrogen forms a total bond order of 1.632, primarily bonding with cerium atoms. In contrast, boron forms a total bond order of 1.807, but it predominantly bonds with oxygen atoms rather than cerium atoms. This difference in bonding behavior can be attributed to the distinct chemical characteristics of nitrogen and boron. Nitrogen is a typical non-metal with strong electronegativity, leading it to form more stable bonds with cerium atoms. On the other hand, boron's non-metallic nature is less pronounced, resulting in a bonding preference with oxygen atoms. The disruption of symmetry and the changes in bonding characteristics due to N and B doping have significant implications for the electronic properties of ceria.

The impact of N and B doping on the electronic properties of ceria was analyzed through the IP, EA, and GEI values of the system (Table 2).

Table 2. Calculated IP, EA and GEI of the studied systems

System	IP, eV	EA, eV	GEI, eV
CeO_2	5.6567	3.3510	4.3987
N/CeO_2	5.6116	3.3014	4.2985
B/CeO_2	5.5060	3.1982	4.1037

The analysis of the results reveals that nitrogen doping decreases the ionization potential and the electron affinity of ceria. Similarly, boron doping results in the reduction of both IP and EA values. These alterations in IP and EA, induced by the incorporation of N and B, lead to significant changes in the global electrophilicity index, which serves as an indicator of the Lewis acidity of the material's surface. Specifically, the GEI for both N/CeO_2 and B/CeO_2 systems shows a decrease when compared to the pristine CeO_2, suggesting a reduction in the Lewis acidity of the ceria surface. This phenomenon can be

attributed to the binding of N and B atoms to the surface Ce atoms, which reduces the number of free Lewis acidic sites available.

The relationship between surface Lewis acidity and the photocatalytic activity of photocatalysts is quite complex and plays a critical role in enhancing photocatalytic performance. Therefore, from a theoretical standpoint, the introduction of non-metallic bases such as N and B does not enhance the photocatalytic activity of ceria through the mechanism of increased surface acidity. This contrasts with the effects observed when doping with transition metals such as Fe [14].

Additionally, various parameters related to the optical properties of the doped materials were calculated. Table 3 and Figure 2 provide a detailed presentation of the calculated values for absolute electronegativity, band gap, energies of the valence band, and conduction band. These values are crucial for understanding the impact of doping on the electronic structure and optical behavior of the materials, further elucidating the effects of N and B doping on ceria's photocatalytic properties.

Table 3. Calculated χ, Eg, E_{VB}, and E_{CB} of the studied systems

System	χ, eV	E_g, eV	E_{VB}, eV	E_{CB}, eV
CeO_2	4.5039	3.1809	1.5939	-1.5862
N/CeO_2	4.4565	2.9563	1.4365	-1.5235
B/CeO_2	4.3521	2.6674	1.1821	-1.4779

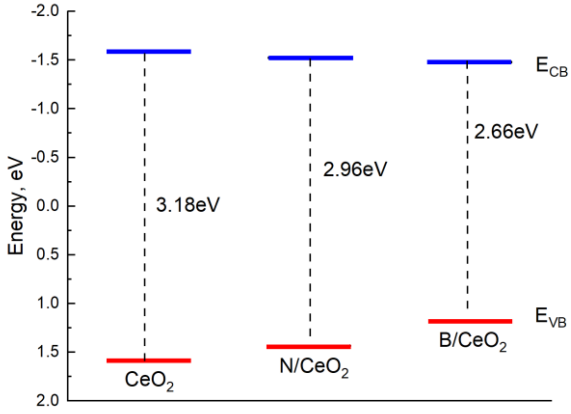

Figure 2. Relative positions of the valence and conduction band energies of CeO_2, N-doped CeO_2, and B-doped CeO_2

The absolute electronegativity and band gap values of pristine ceria are higher compared to those of the N- and B-doped systems. The reduction in the band gap for N/CeO_2 and B/CeO_2 enhances their ability to absorb visible light, which is a critical factor in the design of photocatalytic materials. Since visible light constitutes a significant portion of the solar spectrum, the ability to utilize this light more effectively can significantly improve photocatalytic efficiency. In addition to reducing the band gap, doping with N and B also alters the energetic positions of the valence and conduction bands. Specifically, the presence of N and B results in a decrease (in magnitude) in both the valence band potential and the conduction band potential. This trend is consistent with

the effects observed when non-metal dopants are introduced into other photocatalysts, such as graphitic carbon nitride [15] and TiO_2 [16]. These shifts are more pronounced in the B-doped system compared to the N-doped system. The changes in the valence and conduction band potentials have significant implications for photocatalytic activity. By narrowing the band edges, N and B doping not only enhance the absorption of visible light but also modify the redox potentials of the photocatalyst.

Figure 3 illustrates the HOMO and LUMO images of CeO_2, N/CeO_2, and B/CeO_2. Understanding the composition of the HOMO and LUMO provides valuable information for analyzing the charge transfer capabilities of the photocatalyst.

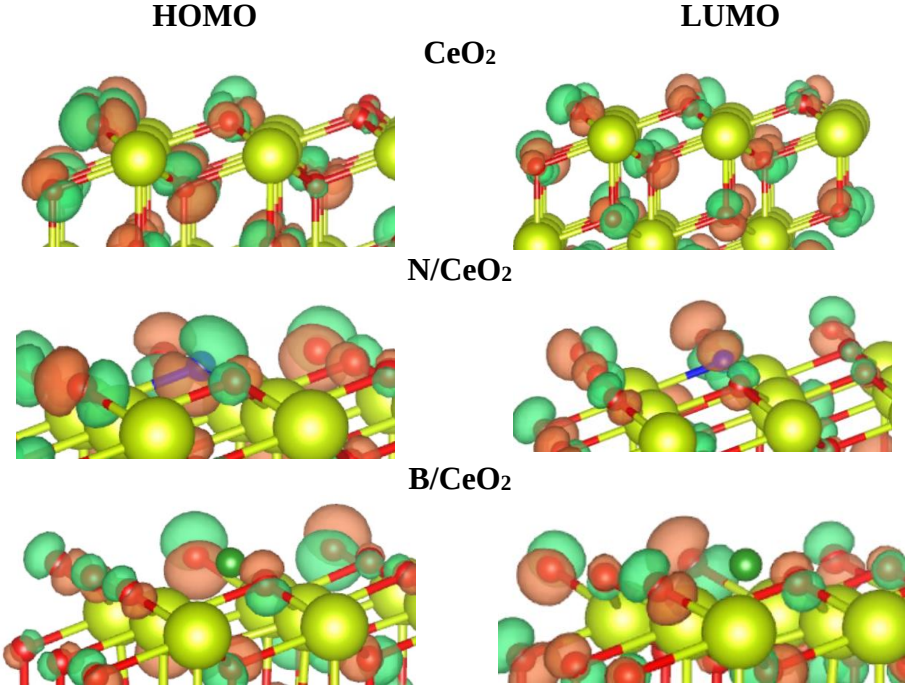

Figure 3. HOMO and LUMO images of CeO_2, N/CeO_2, and B/CeO_2 systems

The HOMO and LUMO orbitals of CeO_2 primarily derive from the oxygen atoms. Upon substitution of oxygen with nitrogen, the p atomic orbitals of nitrogen also contribute to the HOMO and LUMO orbitals in the N/CeO_2 system. However, in the case of B/CeO_2, there is a notable absence of contribution from the p atomic orbitals of boron to the HOMO and LUMO orbitals. This observation suggests a distinct electronic interaction between boron and the CeO_2 matrix compared to nitrogen doping.

It is important to note that during light absorption by a photocatalyst, electron transitions may occur not only between the HOMO and LUMO orbitals but also involving other molecular orbitals with varying energy levels. Therefore, a comprehensive evaluation of UV-VIS spectra is essential to understand the optical properties and potential charge transfer mechanisms. However, the computation of UV-VIS spectra for the studied systems is challenging due to the presence of cerium with 4f subshell electrons, which complicates the electronic structure calculations. Further theoretical and experimental investigations are warranted to overcome these challenges and accurately predict the optical properties of N- and B-doped CeO_2 systems.

3. Conclusions

In summary, employing the DFT+U method in conjunction with the GFN-xTB method, the structural configurations of CeO_2, N-doped CeO_2, and B-doped CeO_2 materials were optimized. The computational results reveal significant alterations in the electronic structure, surface acidity, bandgap, and band edges due to the presence of nitrogen and boron dopants. These findings provide valuable insights for understanding the photocatalytic performance of CeO_2-based materials and offer guidance for future experimental studies and applications in various fields, including environmental remediation and energy conversion processes.

***Acknowledgments*.** This work is funded by the Ministry of Education and Training under grant No. B2022-TDV-06.

REFERENCES

[1] Fauzi A, Jalil A, Hassan N, Aziz F, Azami, Hussain I, Saravanan R & Vo DV, (2022). A critical review on the relationship of CeO_2-based photocatalyst towards mechanistic degradation of organic pollutants. *Chemosphere*, 286, 131651. https://doi.org/10.1016/j.chemosphere.2021.131651.

[2] Tran DP, Pham MT, Bui XT, Wang YF & You SJ, (2022). CeO_2 as a photocatalytic material for CO_2 conversion: A review. *Solar Energy*, 240, 443-466. https://doi.org/10.1016/j.solener.2022.04.051.

[3] Mohanty BC, Lee JW, Yeon DH, Jo YH, Kim JH & Cho YS, (2011). Dopant induced variations in microstructure and optical properties of CeO_2 nanoparticles. *Materials Research Bulletin*, 46(6), 875–883. https://doi.org/10.1016/j.materresbull.2011.02.015.

[4] Abdulwahab KO, Khan MM & Jennings JR, (2023). Doped Ceria Nanomaterials: Preparation, Properties, and Uses. *ACS Omega*, 8(34), 30802-30823. https://doi.org/10.1021/acsomega.3c01199.

[5] Wu C, (2015). Solvothermal synthesis of N-doped CeO_2 microspheres with visible light-driven photocatalytic activity. *Materials Letters*, 139, 382-384. https://doi.org/10.1016/j.matlet.2014.10.127.

[6] Gregori G, Rahmati B, Sigle W, Van Aken PA & Maier J, (2011). Electric conduction properties of boron-doped ceria. *Solid State Ionics*, 192(1), 65-69. https://doi.org/10.1016/j.ssi.2010.07.020.

[7] Han R, Qi M, Mao Z, Lin X & Wu P, (2020). The electronic structure, magnetic and optical properties of B-doped CeO_2 (111) surface by first-principles. *Physics Letters. A*, 384(22), 126526. https://doi.org/10.1016/j.physleta.2020.126526.

[8] Sayyed SAAR, Beedri NI, Kadam VS & Pathan HM, (2016). Rose bengal-sensitized nanocrystalline ceria photoanode for dye-sensitized solar cell application. *Bulletin of Materials Science/Bulletin of Materials Science*, 39(6), 1381-1387. https://doi.org/10.1007/s12034-016-1279-7.

[9] Perdew JP, Burke & Ernzerhof M, (1996). Generalized Gradient Approximation Made Simple. *Physical Review Letters*, 77(18), 3865-3868. https://doi.org/10.1103/physrevlett.77.3865.

[10] Hamann DR, Schlüter M & Chiang C, (1979). Norm-Conserving Pseudopotentials. *Physical Review Letters*, 43(20), 1494-1497. https://doi.org/10.1103/physrevlett.43.1494.

[11] Dudarev SL, Botton GA, Savrasov SY, Humphreys CJ & Sutton AP, (1998). Electron-energy-loss spectra and the structural stability of nickel oxide: An LSDA+U study. *Physical Review. B, Condensed Matter*, 57(3), 1505-1509. https://doi.org/10.1103/physrevb.57.1505.

[12] Grimme S, Antony J, Ehrlich S & Krieg H, (2010). A consistent and accurate ab initio parametrization of density functional dispersion correction (DFT-D) for the 94 elements H-Pu. *Journal of Chemical Physics*, 132(15). https://doi.org/10.1063/1.3382344.

[13] Grimme S, Bannwarth C & Shushkov P, (2017). A Robust and Accurate Tight-Binding Quantum Chemical Method for Structures, Vibrational Frequencies, and Noncovalent Interactions of Large Molecular Systems Parametrized for All spd-Block Elements (Z = 1–86). *Journal of Chemical Theory and Computation*, 13(5), 1989-2009. https://doi.org/10.1021/acs.jctc.7b00118.

[14] Zhang X, Wang J, Song Z, Zhao H, Xing Y, Zhao M, Zhao J, Ma Z, Zhang P & Tsubaki N, (2019). Promotion of surface acidity and surface species of doped Fe and SO_4^{2-} over CeO_2 catalytic for NH3-SCR reaction. *Molecular Catalysis*, 463, 1-7. https://doi.org/10.1016/j.mcat.2018.11.002.

[15] Hussain A, Ali N, Ali SS, Hou J, Aslam I, Naeem H, Boota M, Ul-Hussan M, Yin J & Wang X, (2022). Diverse morphological study for nonmetal-doped g-C_3N_4 composites with narrow bandgap for improved photocatalytic activity. *Research on Chemical Intermediates*, 48(7), 2857-2870. https://doi.org/10.1007/s11164-022-04750-5.

[16] Lu J, Jin H, Dai Y, Yang K & Huang B, (2012). Effect of Electronegativity and Charge Balance on the Visible-Light-Responsive Photocatalytic Activity of Nonmetal Doped Anatase TiO_2. *International Journal of Photoenergy*, 2012, 1-8. https://doi.org/10.1155/2012/928503.